energies

Article

Experimental Optimization of the Compound Angled Asymmetric Laidback Fan Shaped Film Cooling Hole

Ye Rim Jo, Jin Young Jeong and Jae Su Kwak *

School of Aerospace and Mechanical Engineering, Korea Aerospace University, Goyang 10540, Korea
* Correspondence: jskwak@kau.ac.kr

Abstract: In this study, the effect of shape variables on the film cooling effectiveness of the compound angled asymmetric laidback fan shaped hole was experimentally investigated, and the optimum values of select design variables were presented. Among the shape variables of the compound angled asymmetric laidback fan shaped hole, the windward and leeward lateral expansion angles and the compound angle were selected as design variables. Test points were chosen using the central composite design method, and the selected design variables were optimized using the Kriging model. The film cooling effectiveness was measured using the PSP technique, and the experiment was conducted under the two density ratios of 1.5 and 2.0 and four blowing ratios of 1.0, 1.5, 2.0, and 2.5. Experimental results showed that the film cooling performance was improved for higher density ratios than lower density ratios. The main effects analysis indicated that larger windward and leeward lateral expansion angles induced higher film cooling effectiveness; however, the compound angle did not show consistent results. For the optimized hole at the density ratio 2.0, the results indicated that the overall averaged film cooling effectiveness of the optimized compound angled asymmetric laidback fan shaped hole was higher than that of the optimized fan shape holes of previous literature.

Keywords: gas turbine; film cooling; asymmetric laidback fan shaped hole; compound angle; shape optimization

check for updates

Citation: Jo, Y.R.; Jeong, J.Y.; Kwak, J.S. Experimental Optimization of the Compound Angled Asymmetric Laidback Fan Shaped Film Cooling Hole. *Energies* **2022**, *15*, 7985. https://doi.org/10.3390/en15217985

Academic Editors: Ciro Aprea, Adrián Mota Babiloni, Rodrigo Llopis, Jaka Tušek, Angelo Maiorino, Andrej Žerovnik and Juan Manuel Belman-Flores

Received: 21 September 2022
Accepted: 24 October 2022
Published: 27 October 2022

1. Introduction

Turbine inlet temperatures are continuously increasing to achieve the high efficiency of modern gas turbines, resulting in high thermal stress and thermal load on turbine components. Therefore, a sophisticated cooling mechanism must be applied to satisfy the required life of turbine high temperature components.

The film cooling technique is a typical external cooling method for turbine blades, and many researchers have been conducting various studies on the optimization film cooling hole to improve the film cooling effectiveness (FCE). The cylindrical hole, which appeared in the early stages, has the advantage of being simple in structure and easy to manufacture. Goldstein et al. [1], Sinha et al. [2], and Pedersen et al. [3] studied the behavior of coolant injected through cylindrical holes with various flow conditions. However, the cylindrical hole is characterized by the decrease in FCE at the high blowing ratio due to the lift-off of coolant. Fan shaped holes were suggested to alleviate the coolant lift-off and increase the FCE. Chen et al. [4] compared the FCE of four different holes (simple angled cylindrical hole, compound angled cylindrical hole, simple angled fan shaped hole, and compound angled fan shaped hole) at different density ratio, blowing ratio, and turbulence intensity conditions. Their results showed that the fan shaped hole diffused the coolant more uniformly than the cylindrical hole and induced a low coolant momentum at the hole exit, which results in higher and more uniform FCE. Yang et al. [5] proposed three new hole shapes: a bean shaped hole, clover shaped hole, and winter sweet-shaped hole to improve film cooling performance and compared them with the cylindrical hole. In addition, many researchers have suggested various hole shapes to increase FCE, such as anti-vortex holes for offsetting the kidney vortex [6,7], and the holes with trench [8,9] and vortex generator [10,11] and triangular tabs [12].

Due to the shape of gas turbine blades and the limitation in the hole manufacturing process, some film cooling holes inevitably have compound angles. Film cooling with compound angled round holes were considered by Schmidt et al. [13], and they showed that the compound angled round hole significantly improved the film cooling performance. Ekkad et al. [14] conducted experimental studies on the effects of compound angles on cylindrical holes using the transient liquid crystal technique, and Zamiri et al. [15] reported numerical studies using large eddy simulation (LES) on the effect of a compound angled fan shaped hole. They demonstrated that the compound angled holes improved the film cooling performance by providing a large coolant coverage region. Moreover, Huang et al. [16] investigated FCE and heat transfer performance of simple and compound cylindrical holes in transverse trenches, and Bashir et al. [17] studied FCE by changing the arrangement and compound angle, and their results showed that three rows of compound holes in a staggered arrangement resulted in higher film cooling performance due to the better film coverage. Natsui et al. [18]. investigated four arrays of film cooling holes and found that compound angle arrays of cylindrical holes could provide significant levels of FCE at the large spacing.

In general, a lateral expansion angle, one of the major shape variables of the laidback fan shaped hole, is designed symmetrically for uniform coolant diffusion. However, if a compound angle is applied to the fan shaped hole, the lateral expansion angle in the windward and leeward directions should be considered independently to derive optimal shape.

Many studies, including Lee et al. [19,20] and Seo et al. [21], have been conducted to optimize the shape of the film cooling holes, but most of them were conducted by numerical methods and had not considered asymmetrical lateral expansion angles. In this study, the optimization of the compound angled asymmetric laidback fan shaped hole shown in Figure 1 was conducted using an experimental approach. Windward (γ_{ww}) and leeward (γ_{lw}) lateral expansion angles, and the compound angle (θ) were selected as design parameters, and four blowing ratios and two density ratios were considered. The effects of those parameters on the FCE are discussed.

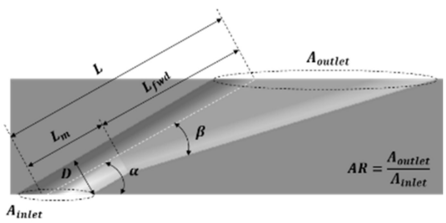

(**a**)

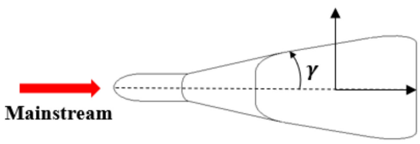

(**b**)

Figure 1. *Cont.*

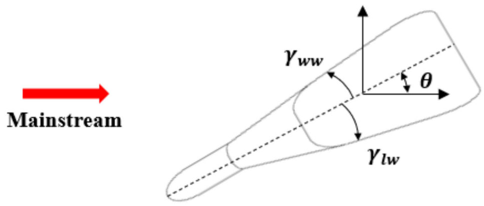

(**c**)

Figure 1. Geometry of the compound angled asymmetric laidback fan shaped hole: (**a**) laidback fan shaped hole; (**b**) simple angled symmetric laidback fan shaped hole; (**c**) compound angled asymmetric laidback fan shaped hole.

2. Measurement Theory and Test Apparatus

2.1. PSP (Pressure Sensitive Paint) Technique

The pressure sensitive paint (PSP) technique was applied to measure the FCE. The PSP technique is the mass transfer technique commonly used in previous studies because it has the advantage of measuring the distribution of FCE with little error due to thermal conduction. The PSP (Uni-FIB 400, ISSI) used in this study is a commercial product and was sprayed on the test plate. When the PSP coated surface is irradiated by light of 400 nm wavelength, the luminescent molecules in the PSP enter an excited state and then return to the ground state by emitting long wavelengths of 600 nm. Using these characteristics, the partial pressure of oxygen on the PSP coated surface can be calculated by measuring the emitting intensity of the PSP. The relationship between the emitted intensity and the oxygen partial pressure can be expressed as Equation (1).

$$\frac{P_{O_2}}{P_{O_2,ref}} = A(T) + B(T)\left(\frac{I_{ref} - I_{blk}}{I - I_{blk}}\right) + \ldots \tag{1}$$

In Equation (1), I and P_{O_2} are respectively the emitted intensity and partial pressure of oxygen. Subscript ref means reference condition, where LED is irradiated and the wind tunnel is turned off, and *blk* means black condition, where the LED and wind tunnel are turned off. I_{blk} is intended to consider the noise of the camera sensor and subtracted from all captured images. $A(T)$ and $B(T)$ are the coefficients obtained from the PSP calibration test, which are expressed as a function of the temperature.

Figure 2 shows the relation between the PSP emitting intensity and the pressure. The calibration was performed by installing a PSP coated plate in the vacuum chamber at the same temperature condition with the film cooling measurement tests. Using the PSP calibration curve, the relation between PSP intensity and pressure ratio is obtained, and then, the FCE can be calculated using Equation (2) [4].

$$\eta = 1 - \frac{1}{\left(\frac{P_{O_2,air}/P_{O_2,ref}}{P_{O_2,fg}/P_{O_2,ref}} - 1\right)\frac{\omega_{fg}}{\omega_{air}} + 1} \tag{2}$$

Here, $\frac{\omega_{fg}}{\omega_{air}}$ is the density ratio between the foreign gas and air. Detailed descriptions of PSP are presented in Han et al. [4].

2.2. Geometry of the Compound Angled Asymmetric Laidback Fan Shaped Film Cooling Hole

The reference film cooling hole was selected based on the optimized laidback fan shaped hole by Seo et al. [21]. The hole diameter (D) and the hole length to diameter ratio (L/D) were 1.5 mm and 6, respectively, and the injection angle (α) and the forward expansion angle (β) were fixed at 30 degrees and 13.3 degrees, respectively. For optimization, the windward (γ_{ww}) and leeward (γ_{lw}) lateral expansion angles and compound angle (θ) were selected as design variables. Table 1 presents the lower and upper limits of the shape variables. A detailed description of the shape variables is given in Figure 1.

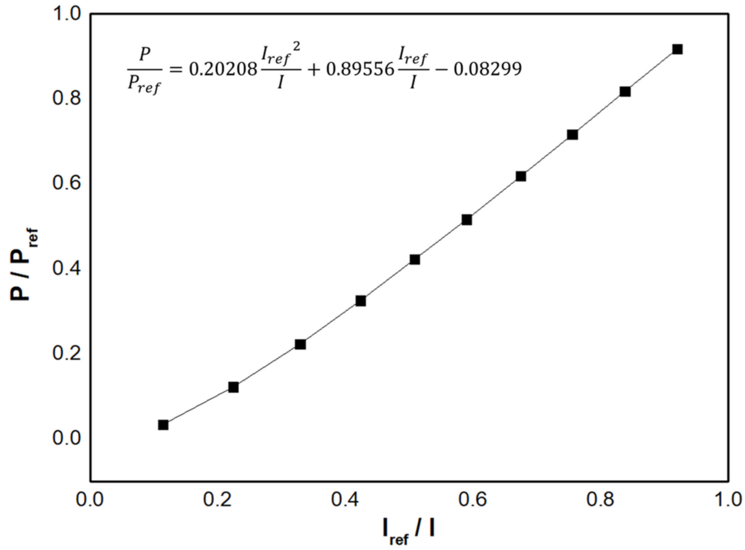

Figure 2. PSP calibration curve.

Table 1. Design variables of optimization.

Shape Variable	Lower Limit	Upper Limit
Windward lateral expansion angle (γ_{ww})	0°	15°
Leeward lateral expansion angle (γ_{lw})	0°	15°
Compound angle (θ)	0°	30°

2.3. Test Facility

Figure 3 is the schematic of an experimental setup for measuring FCE and the test facility was the same as one used by Park et al. [22]. They compared their results with those of previous studies with similar hole configurations and demonstrated good agreement with the references. Test plates were manufactured using the SLA (Stereolithography Apparatus) 3D printing technique with a layer thickness of 0.05 mm, and the plate was installed on the plenum chamber with screen meshes and a honeycomb layer. All test plates had three identical holes, each with a hole pitch of 10D.

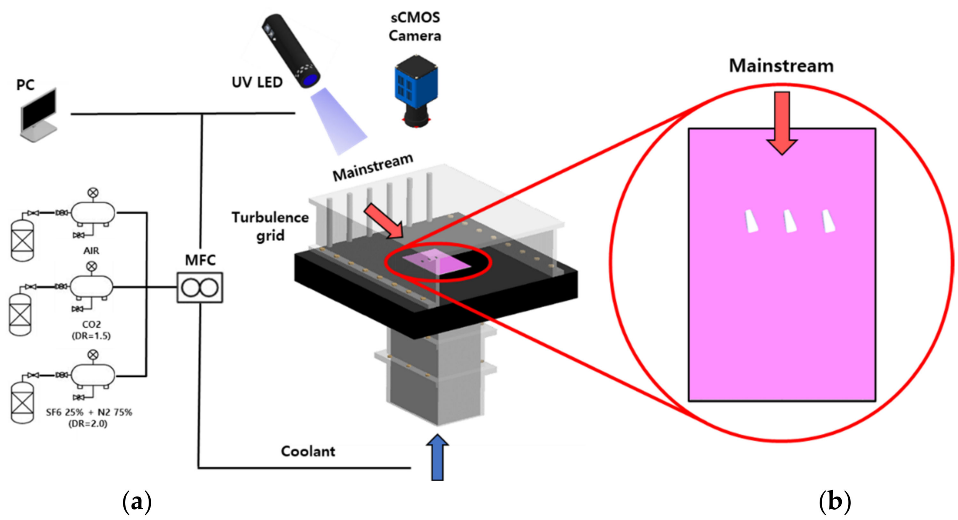

Figure 3. Schematic of the film cooling test apparatus: (**a**) test section; (**b**) test plate.

The mainstream velocity was 20 m/s; the turbulence grid with a diameter of 10 mm was installed 200 mm upstream from the hole exit, and the resulting mainstream turbulence intensity was 12%. The boundary layer thickness was 5mm at 30 mm upstream from the hole exit. Carbon dioxide (CO_2) and gas mixture of Nitrogen and Sulfur hexafluoride (75% N_2 + 25% SF_6) were used as coolant to simulate density ratios of 1.5 and 2.0. Flow rates were controlled using a mass flow controller (FMA-2600 series, Omega), and the blowing ratios were tested under conditions of 1.0, 1.5, 2.0, and 2.5.

To measure the FCE, a test plate coated with the PSP (Uni-FIB 400, ISSI) was installed on the test section. Air-cooled LED (LM2X-DM-400, ISSI) for irradiating light of 400 nm was installed on the test section, and the emission intensity of the PSP was measured using an sCMOS camera (PCO edge 3.1, PCO).

In this study, the uncertainty of measuring the film cooling efficiency using the PSP technique was estimated as ±8% for η = 0.3, and ±1.5% for η = 0.7 [23].

3. Shape Optimization

3.1. Design of Experiment

The central composite design method was applied to choose test points. Despite a relatively large number of test cases, the central composite design method has an advantage in analyzing the effect of the design variables [24]. The objective function for optimization was defined as the overall averaged FCE estimated over the area within 30D in the streamwise direction and ±5D in the pitchwise direction from the center of the cylinder part of the hole following the definition by Brauckmann et al. [25] as shown in Figure 4. Table 2 shows test points obtained by the central composite design method for three design variables.

For the convenience of designation, the compound angled asymmetric laidback fan shaped hole was named using three angles: $\gamma_{ww} - \gamma_{lw} - \theta$.

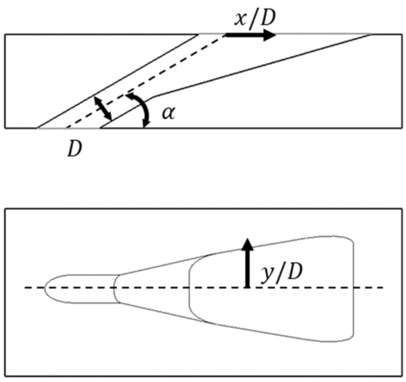

(**a**)

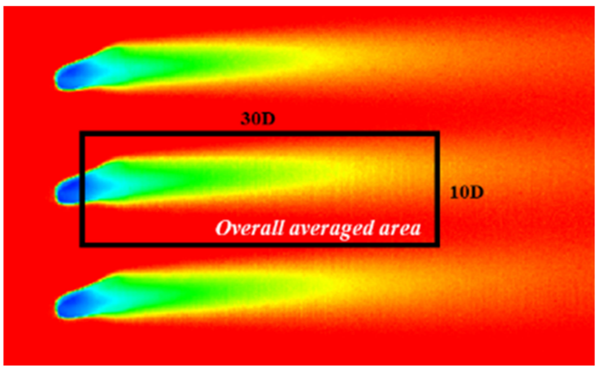

(**b**)

Figure 4. Definition of coordinate and overall averaged area of the compound angled asymmetric fan shaped hole: (**a**) definition of coordinate; (**b**) overall averaged area.

Table 2. Test matrix obtained by using the central composite design method.

Case No.	Windward Lateral Expansion Angle	Leeward Lateral Expansion Angle	Compound Angle
Case 1	11.96°	11.96°	6.08°
Case 2	3.04°	3.04°	6.08°
Case 3	3.04°	11.96°	6.08°
Case 4	11.96°	3.04°	6.08°
Case 5	11.96°	3.04°	23.92°
Case 6	11.96°	11.96°	23.92°
Case 7	3.04°	3.04°	23.92°
Case 8	3.04°	11.96°	23.92°
Case 9	0°	7.5°	15°
Case 10	15°	7.5°	15°
Case 11	7.5°	7.5°	0°
Case 12	7.5°	7.5°	30°
Case 13	7.5°	15°	15°
Case 14	7.5°	0°	15°
Case 15	7.5°	7.5°	15°

3.2. Kriging Model

In this study, the Kriging model was used to obtain optimal objective function. The Kriging model method is an approximate model technique that finds the distribution at unknown points using sample points already calculated using random variables to determine the correlation of the data. The Kriging model method is flexible in modeling nonlinear design problems and has a high degree of approximation accuracy even if the range of design variables is slightly larger. The unknown function to be approximated is defined as $\hat{y}$, which is expressed mathematically as shown in Equation (3) using two element models.

$$\hat{y} = f(x) + Z(x) \tag{3}$$

Here, $f(x)$ is a globalized model represented by a constant term, and x is a vector composed of design variables. $Z(x)$ is a Gaussian random function with an average of zero and a covariance, which corrects the difference between the actual experimental value and the global model.

The covariance of $Z(x)$ to determine the correlation of random variables is expressed as Equation (4). Here, $\boldsymbol{R}$ is a correlation matrix expressed by the correlation function $R(x_i, x_j)$ between two points x_i, x_j given by some sample data.

$$Cov(x_i, x_j) = \sigma^2 \boldsymbol{R}[R(x_i, x_j) \tag{4}$$

The predicted function by the kriging model, where the square error is minimized, is expressed as below in Equation (5) [26,27].

$$\hat{y}(x) = f^T(x)\hat{\beta} + r^T(x)R^{-1}(\boldsymbol{Y} - \boldsymbol{F}\hat{\beta}) \tag{5}$$

4. Results and Discussion

4.1. Distributions of Film Cooling Effectivenes

Figure 5 shows the distribution of FCE for all tested cases, and it is clearly seen that the FCE was significantly affected by the hole shape. In general, higher FCE was observed for higher density ratio cases (DR = 2.0), but the effect of blowing ratio on the FCE was not consistent. In addition, the holes with larger AR resulted in higher FCE. It seems that the coolant was diffused uniformly due to the large outlet area. However, the case with relatively large AR and compound angles (i.e., cases 5, 6, 10, and 12) showed coolant separation near the windward side of the hole exit due to a relatively large coolant flow angle with respect to the mainstream flow. The coolant separation at the hole windward side was more significant for lower blowing ratio cases.

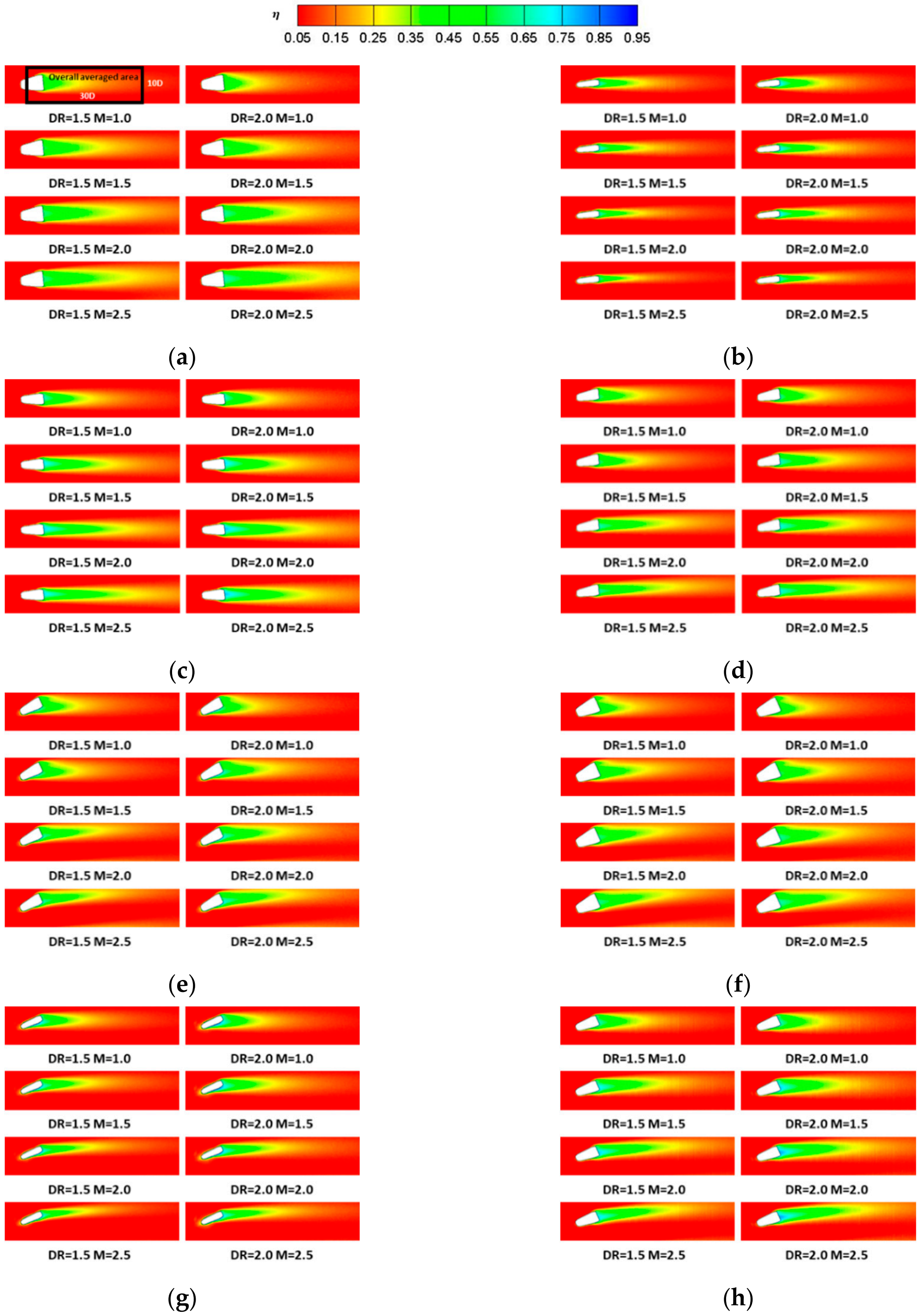

Figure 5. Cont.

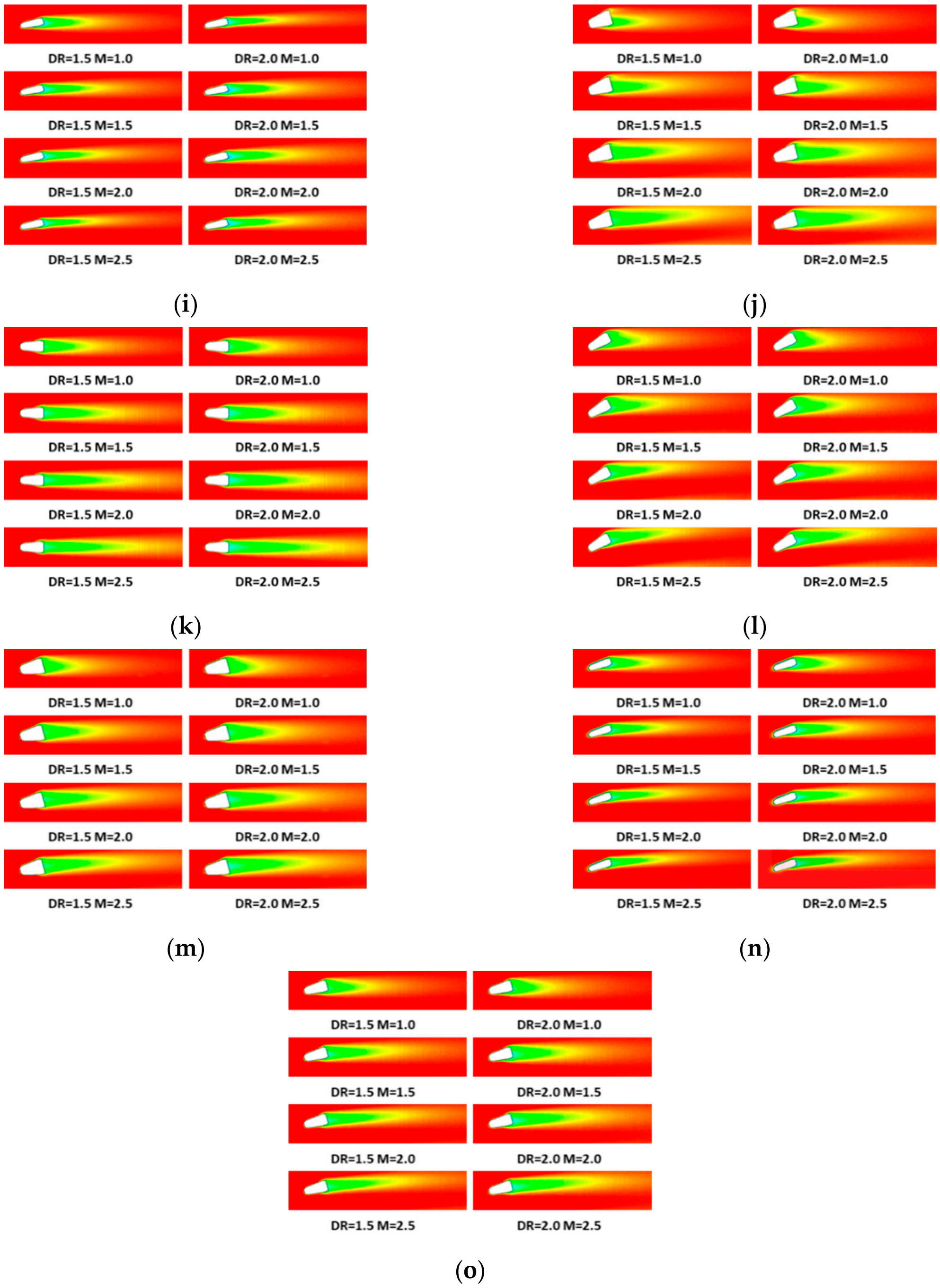

Figure 5. Distribution of the FCE: (**a**) Case 1 (11.96-11.96-6.08); (**b**) Case 2 (3.04-3.04-6.08); (**c**) Case 3 (3.04-11.96-6.08); (**d**) Case 4 (11.96-3.04-6.08); (**e**) Case 5(11.96-3.04-23.92); (**f**) Case 6 (11.96-11.96-23.92); (**g**) Case 7 (3.04-3.04-23.92); (**h**) Case 8 (3.04-11.96-23.92); (**i**) Case 9 (0-7.5-15); (**j**) Case 10 (15-7.5-15); (**k**) Case11 (7.5-7.5-0); (**l**) Case 12 (7.5-7.5-30); (**m**) Case 13 (7.5-15-15); (**n**) Case 14 (7.5-0-15); (**o**) Case 15 (7.5-7.5-15).

4.2. Effects of Asymmetric Lateral Expansion Angle

Figure 6 presents the overall averaged FCE for the cases with the same compound angle but mirror-image shape, where the windward lateral expansion angle (γ_{ww}) of one hole is the same as the leeward lateral expansion angle (γ_{lw}) of the other hole. As mentioned above, the higher density ratio cases provided better FCE than the lower density ratio cases, but the effect of the blowing ratio was not consistent.

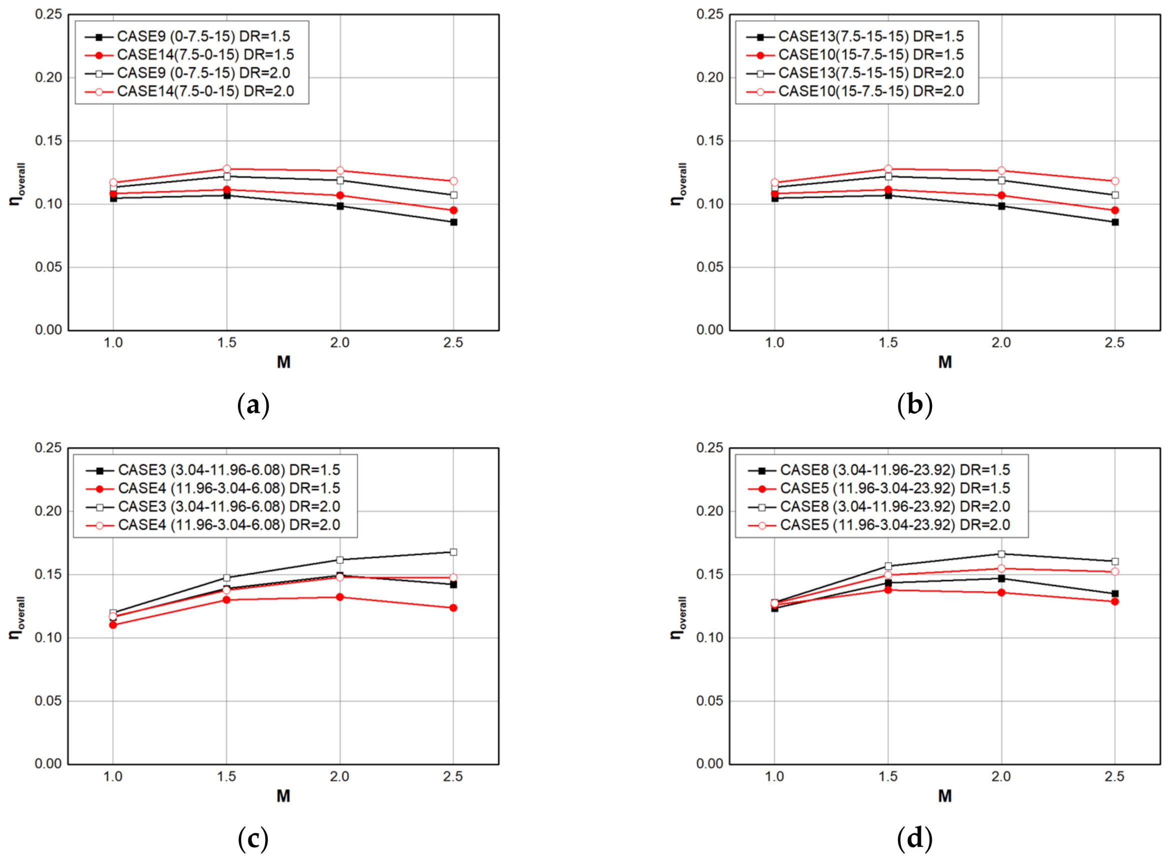

Figure 6. Overall averaged FCE for the effects of asymmetric lateral expansion angle: (**a**) (0-7.5-15) and (7.5-0-15) holes; (**b**) (7.5-15-15) and (15-7.5-15) holes; (**c**) (3.04-11.96-6.08) and (11.96-3.04-6.08) holes; (**d**) (3.04-11.96-23.92) and (11.96-3.04-23.92) holes.

Figure 6a,b indicate that the larger windward lateral expansion angle results in higher FCE; however, Figure 6c,d show a reverse trend.

Therefore, it can be said that the effects of asymmetric lateral expansion angle on the FCE did not have a consistent trend but were coupled with the compound angle.

4.3. Effects of the Windward Lateral Expansion Angle

The effects of the windward lateral expansion angle on the distribution of the FCE can be observed if we compare the cases with the same leeward lateral expansion angle and compound angle but different windward lateral expansion angles (i.e., Case 9 (0-7.5-15, Figure 5i), Case 15 (7.5-7.5-15, Figure 5o), and Case 10 (15-7.5-15, Figure 5j). Those cases have the same leeward lateral expansion angle (7.5°) and compound angle (15°), but the windward lateral expansion angle varies from 0° to 15°.

For Case 10 (15-7.5-15, Figure 5j) which has a larger windward lateral expansion angle and larger hole exit area, the coolant separated from the windward side of the hole at the lower blowing ratios. For higher blowing ratios, as the coolant momentum increased, the coolant separation at the location was not observed, and relatively uniform and high FCE was observed. In contrast, Case 9 (0-7.5-15, Figure 5i) which has a smaller windward lateral expansion angle and smaller hole exit area, coolant separation was not observed even for the lower blowing ratio cases; however, overall FCE was lower for Case 9. Higher coolant momentum for Case 9 prevented the coolant separation near the windward side of the hole exit but induced the coolant lift off and reduced coolant diffusion, resulting in relatively low FCE.

Figure 7 presents the overall averaged FCE for cases with the same leeward lateral expansion and the same compound angle, but different windward lateral expansion angles (γ_{ww}-11.96-6.08, γ_{ww}-3.04-6.08, γ_{ww}-3.04-23.92, γ_{ww}-11.96-23.92, and γ_{ww}-7.5-15).

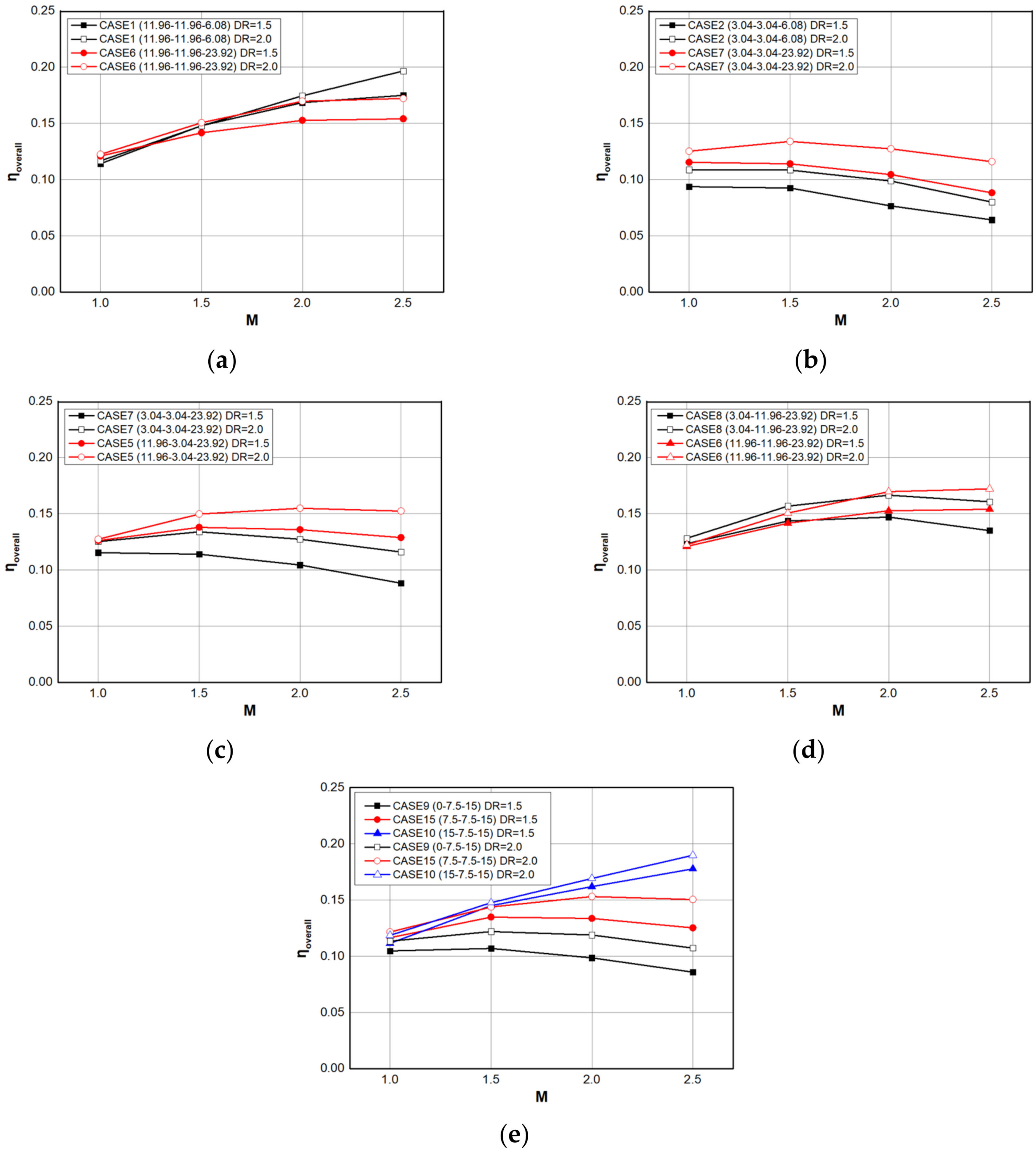

Figure 7. Overall averaged FCE for the effect of windward lateral expansion angle: (**a**) γ_{ww}-11.96-6.08 cases; (**b**) γ_{ww}-3.04-6.08 cases; (**c**) γ_{ww}-3.04-23.92 cases; (**d**) γ_{ww}-11.96-23.92 cases; (**e**) γ_{ww}-7.5-15 cases.

All selected combinations of holes showed better film cooling performance at higher density ratios, but the effects of the blowing ratio were not consistent. Generally, cases with larger windward lateral expansion angle showed higher FCE at the higher blowing ratios because of well diffused coolant in the lateral direction. However, in Figure 7d, the FCE of Case 6 (11.96-11.96-23.92) with the larger windward lateral expansion angle was smaller than that of Case 8 (3.04-11.96-23.92) at the low blowing ratios because of the coolant separation near the windward side of the hole exit, as discussed above.

4.4. Effects of the Leeward Lateral Expansion Angle

Case 14 (7.5-0-15, Figure 5n), Case 15 (7.5-7.5-15, Figure 5o), and Case 13 (7.5-15-15, Figure 5 m) were compared to observe the effects of leeward lateral expansion angle. In Case 14 (7.5-0-15, Figure 5n), the coolant was not diffused well due to the higher momentum generated by the relatively narrow hole exit area; however, for Case 13 (7.5-15-15, Figure 5m), FCE was higher due to the larger hole exit area.

Figure 8 presents the overall averaged FCE for the combination of cases with the same windward lateral expansion angle (γ_{ww}) and compound angle (θ), but different leeward lateral expansion angles (γ_{lw}), i.e., (11.96-γ_{lw}-6.08, 3.04-γ_{lw}-6.08, 11.96-γ_{lw}-23.92, 3.04-γ_{lw}-23.92, and 7.5-γ_{lw}-15). Again, all cases show higher FCE at the higher density ratio cases (DR = 2.0), and for each hole shape, the effects of blowing ratio were not consistent. Moreover, in general, FCE is higher for the higher leeward lateral expansion angle cases due to the relatively larger hole exit area and well diffused coolant as mentioned above.

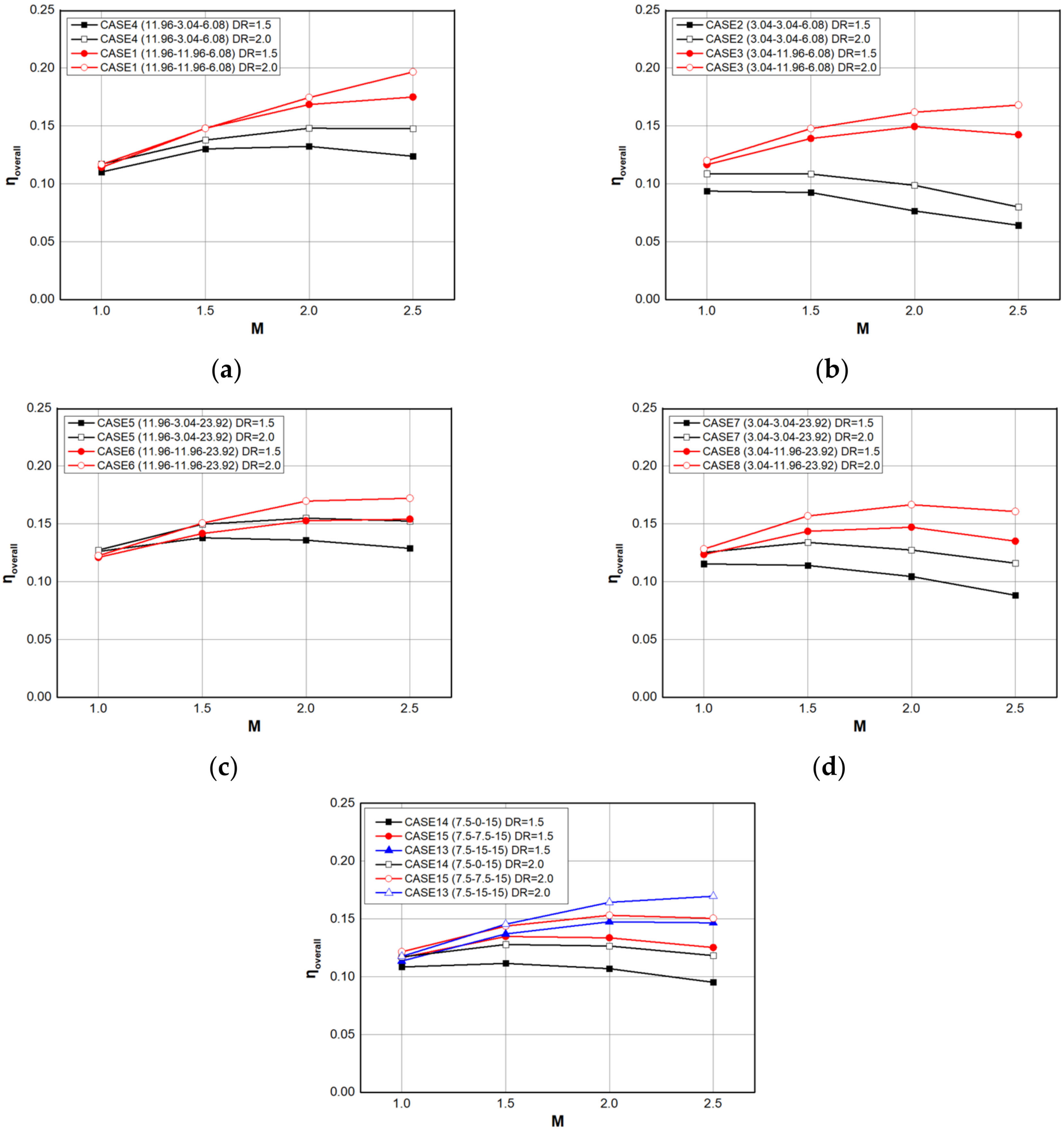

(e)

Figure 8. Overall averaged FCE for the effect of leeward lateral expansion angle: (**a**) 11.96-γ_{lw}-6.08 cases; (**b**) 3.04-γ_{lw}-6.08 cases; (**c**) 11.96-γ_{lw}-23.92 cases; (**d**) 3.04-γ_{lw} -23.92 cases; (**e**) 7.5-γ_{lw}-15 cases.

4.5. Effects of the Compound Angle

Figure 9 presents the overall averaged FCE of hole combinations (11.96-11.96-θ, 3.04-3.04-θ, 3.04-11.96-θ, 11.96-3.04-θ, and 7.5-7.5-θ) to investigate the effect of compound angle (θ). For all cases, higher density ratio resulted in better film cooling performance, but the effects of blowing ratio were not consistent. For each combination of cases, the effect of the compound angle was not consistent. In Figure 9b,d, larger compound angle cases (Case 5 and Case 7) showed higher FCE at all blowing ratios, while other combinations did not show a consistent trend.

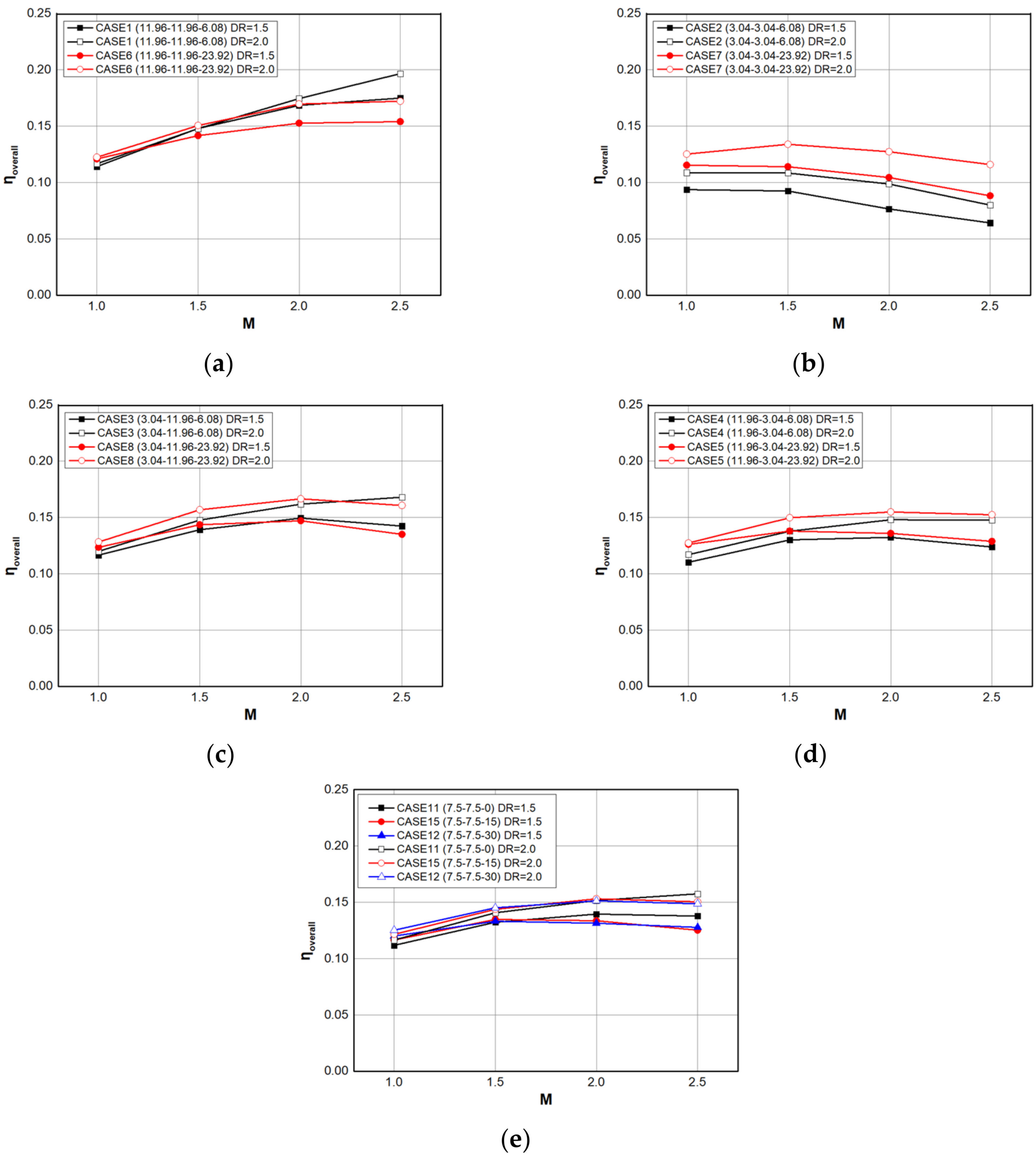

Figure 9. Overall averaged FCE for the effect of compound angle: (**a**) 11.96-11.96-θ cases; (**b**) 3.04-3.04-θ cases; (**c**) 3.04-11.96-θ cases; (**d**) 11.96-3.04-θ cases; (**e**) 7.5-7.5-θ cases.

4.6. Main Effects Analysis

Figure 10 shows the main effect of the design variables at the blowing ratio 2.0 and density ratio 2.0 which are similar to the operating condition of an actual gas turbine. The main effect indicates the effects of change in the design variable on the objective function. Moreover, a larger gradient in the main effect graph means a larger effect upon the variable.

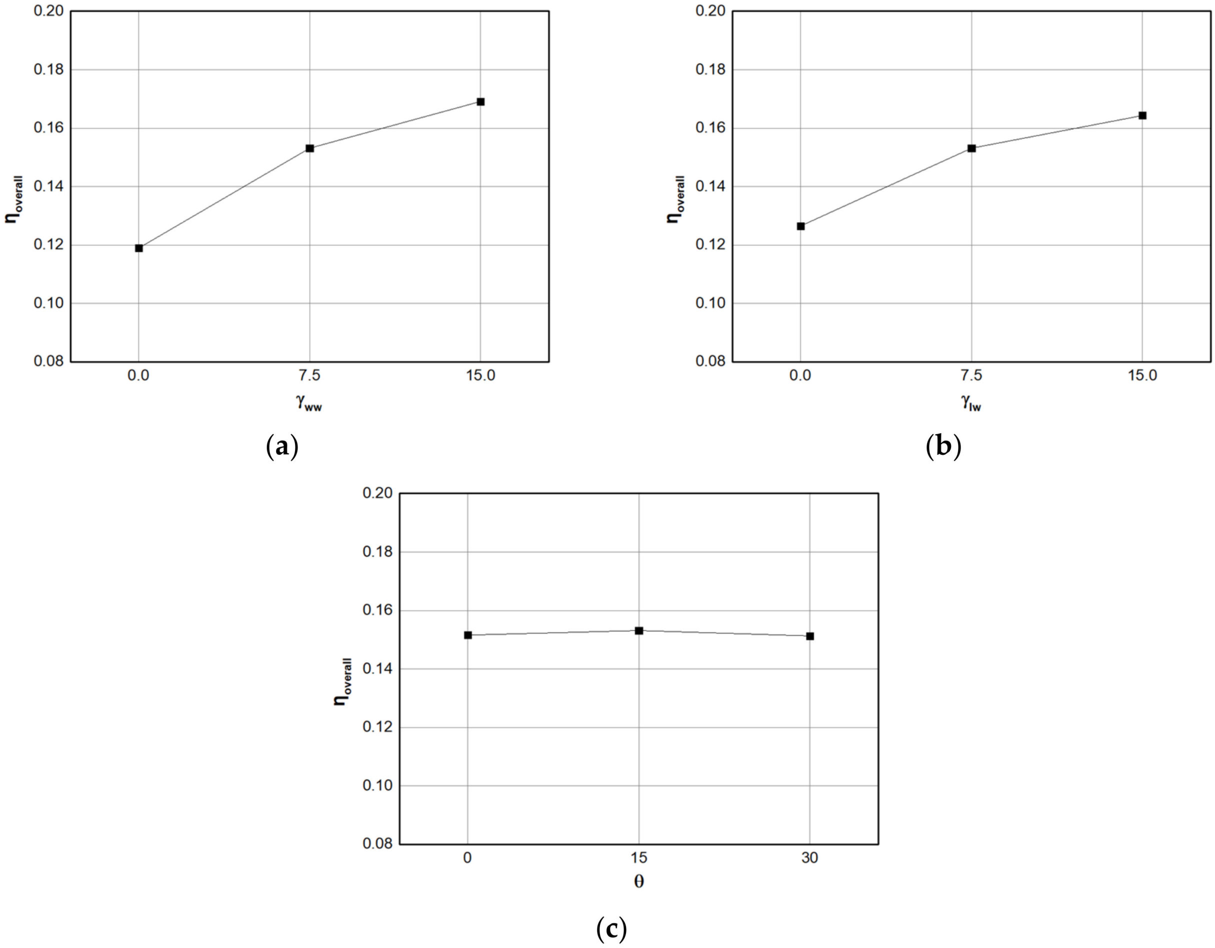

Figure 10. Main effects plots: (**a**) windward lateral expansion angle; (**b**) leeward lateral expansion. angle (**c**) Compound angle.

As shown in Figure 10a,b, the FCE was strongly affected by the windward and leeward lateral expansion angles, and the effect was more significant, with a steeper gradient, for smaller angles. In Figure 10c, the compound angle of 15° showed the highest FCE; however, the effect of the compound angle was relatively small (smaller gradient).

4.7. Overall Averaged FCE

Figure 11 shows the overall averaged FCE for all cases. Higher FCE was observed for the high-density ratio (DR = 2.0) case at the given hole shape, and the effects of blowing ratio were not consistent for each hole. However, the effects of blowing ratio on the FCE for each hole were similar for both density ratios.

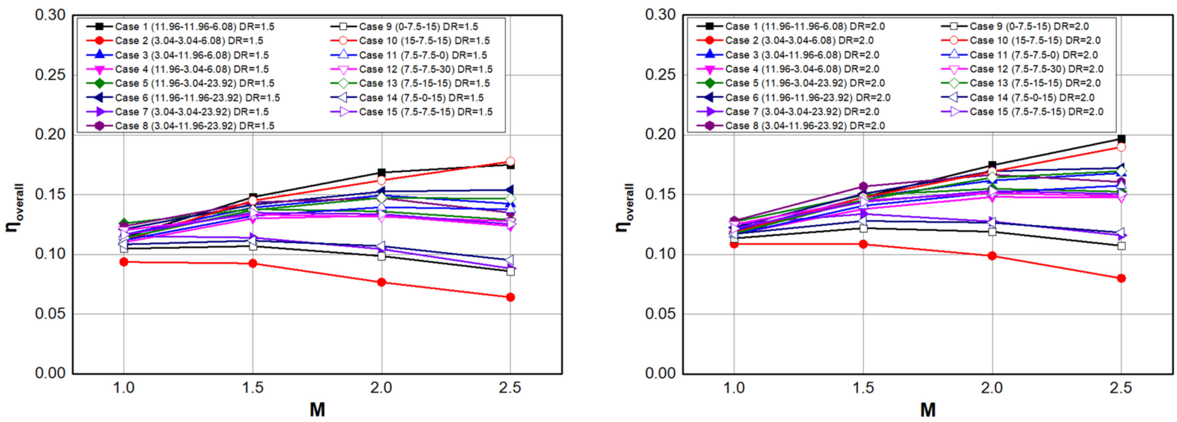

(**a**) (**b**)

Figure 11. Overall averaged FCE for effect for all tested cases: (**a**) DR = 1.5, (**b**) DR = 2.0.

Figure 12a indicates the overall averaged FCE versus the AR. Case 1 (11.96-11.96-6.08), Case 10 (15-7.5-15), and Case 6 (11.96-11.96-23.92) with relatively larger hole exit areas showed high FCE at all density ratios; however, a relatively low FCE was obtained in Case 2 (3.04-3.04-6.08), Case 9 (0-7.5-15), and Case 14 (7.5-0-15) with relatively small hole exit areas. Next, Figure 12b shows overall averaged FCE versus the AR and blowing ratio. In a previous study by Park et al. [27], the overall averaged FCE of fan shaped holes tended to decrease if the AR exceeded the peak point; however, within the considered range of the current study for the compound angled asymmetric laidback fan shaped hole, a larger AR resulted in higher FCE.

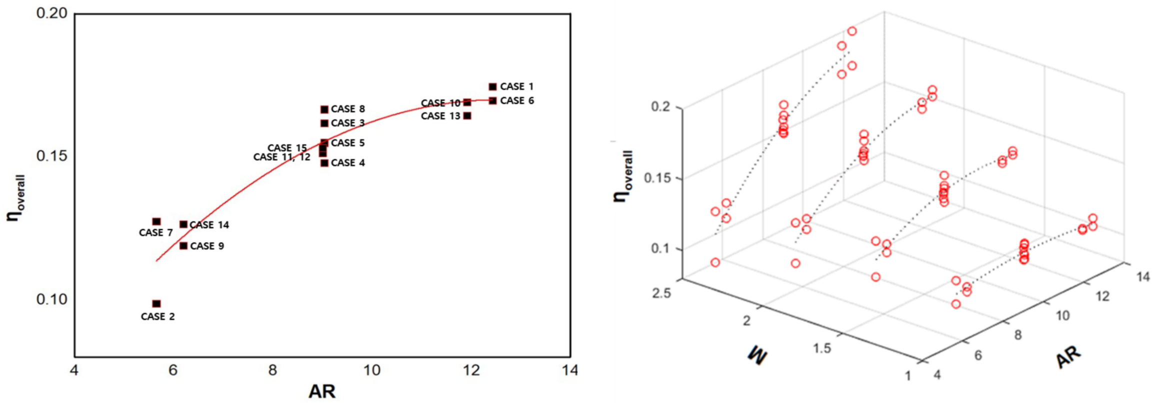

(**a**) (**b**)

Figure 12. Overall averaged FCE: (**a**) versus the AR; (**b**) versus the AR and M.

The effect of the shape variables on the FCE varied depending on all operating environments. Therefore, in this study, the optimization holes with a different shape for each blowing ratio under the density ratio 2.0 which is similar to the operating condition of the actual gas turbine were designed and investigated.

4.8. Result of Optimization

In this study, an optimal hole shape at each blowing ratio was obtained for the density ratio 2.0 condition using the Kriging model. Table 3 presents results of optimization and the predicted overall averaged FCE. As the blowing ratio increased, the optimum compound angle gradually decreased, while the optimum AR gradually increased, and the overall averaged FCE was higher for the higher blowing ratio.

Table 3. Results of the optimized design variables at DR = 2.0.

	Windward Lateral Expansion Angle	Leeward Lateral Expansion Angle	Compound Angle	Area Ratio	$\eta_{overall,opt}$
M = 1.0	5.46	8.33	24.56	8.55	0.129
M = 1.5	3.49	14.7	20.91	10.28	0.159
M = 2.0	3.94	15	11.82	10.57	0.177
M = 2.5	13.49	13.03	5.15	13.44	0.202

Figure 13 shows the optimal hole shapes at different blowing ratios, and the optimized holes were tested again to obtain the FCE. The distribution of FCE for optimized holes was presented in Figure 14, and the comparison between the predicted and the measured overall averaged FCE is shown in Figure 15. The maximum difference between the predicted and the measured FCE was about 5.7%, which signifies that the optimization results were predicted well.

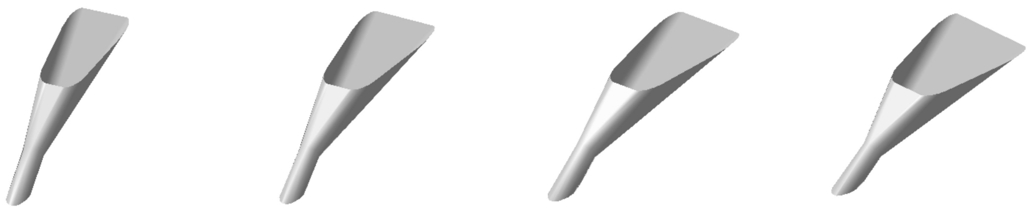

(**a**) (**b**) (**c**) (**d**)

Figure 13. Shapes of optimized asymmetric laidback fan shaped hole at different blowing ratios: (**a**) optimized hole at M = 1.0 (5.46-8.33-24.56); (**b**) optimized hole at M = 1.5 (3.49-14.7-20.91); (**c**) optimized hole at M = 2.0 (3.94-15-11.82); (**d**) optimized hole at M = 2.5 (13.49-13.03-5.15).

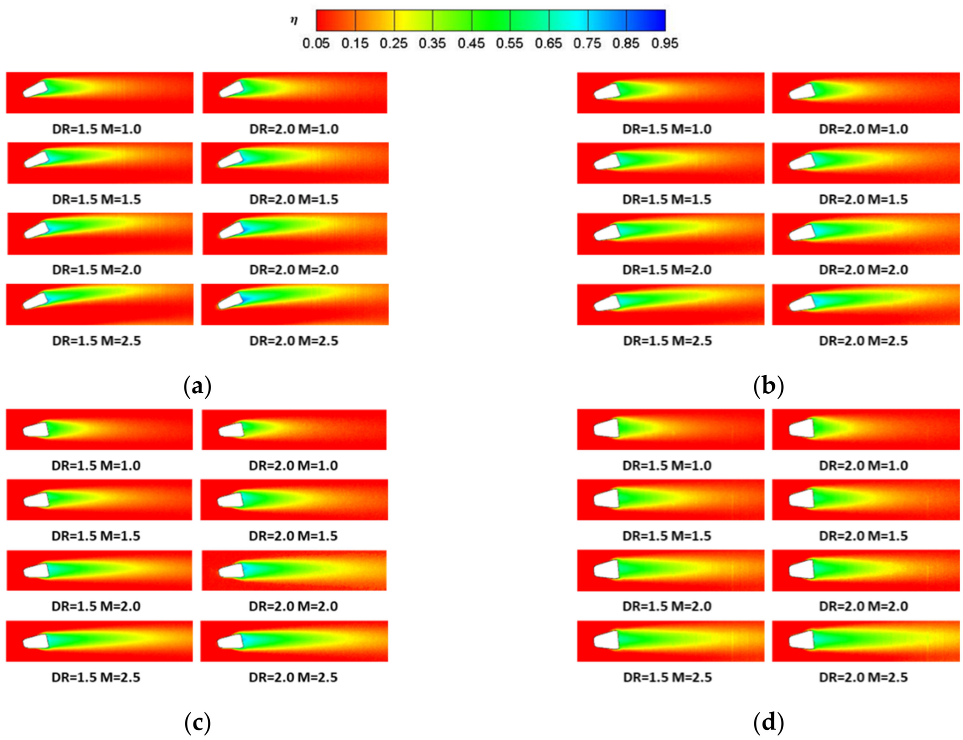

Figure 14. Distribution of optimized asymmetric laidback fan shaped hole (**a**) optimized hole at M = 1.0 (5.46-8.33-24.56); (**b**) optimized hole at M = 1.5 (3.49-14.7-20.91); (**c**) optimized hole at M = 2.0 (3.94-15-11.82); (**d**) optimized hole at M = 2.5 (13.49-13.03-5.15).

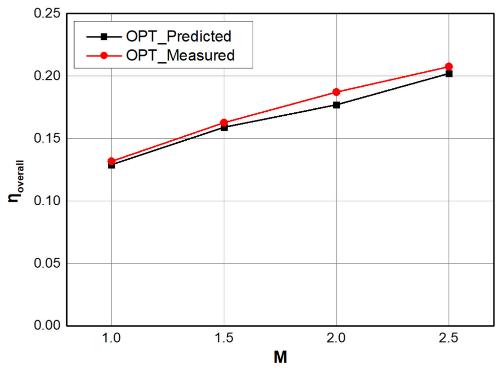

Figure 15. Overall averaged FCE for optimized hole.

Figure 16 presents a comparison of the overall averaged FCE of the optimized holes by Park et al. [28], Seo et al. [21], and the current study at the conditions of the blowing ratio 2.0 and the density ratio 2.0. All three optimized holes had the same injection angle of 30° and the metering length of 2. Results showed that the FCE of the optimized compound angled asymmetric laidback fan shaped hole was higher than that of the experimentally optimized hole [28] and numerically optimized hole [21] by 1.3% and 8%, respectively.

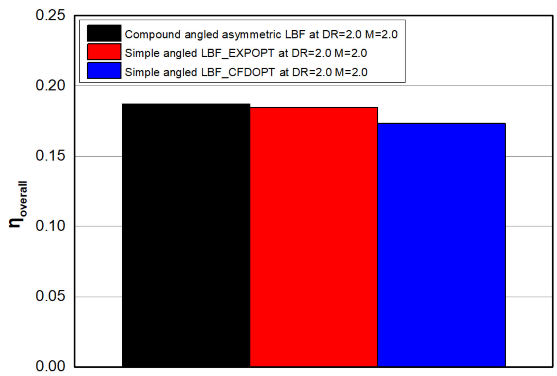

Figure 16. Comparison of FCE in the compound angled asymmetric laidback fan shaped hole and the simple angled symmetric laidback fan shaped hole.

5. Conclusions

In this study, the effect of the compound angled asymmetric fan shaped hole was experimentally investigated using the PSP technique. Among the shape variables of the compound angled asymmetric laidback fan shaped hole, windward lateral expansion angle, leeward expansion angle, and compound angle were selected as design variables. The optimized hole shape was derived using the Kriging model. In addition, the optimized laidback fan shaped hole from previous studies was compared with the optimized hole in this study under the same conditions. The main results of this study are as follows:

(1) The overall FCE of mirror-image shape holes with the same compound angle showed different trends depending on hole shape.
(2) The main effects indicated that the FCE increased as the windward and leeward lateral expansion angles increased, but the effects of the compound angles were not consistent.
(3) The overall FCE was higher at the higher density ratio (DR = 2.0) and the larger AR improved film cooling performance.
(4) The optimal hole shape at each blowing ratio indicated that the compound angle decreased, and the hole exit area widened as the blowing ratio increased.
(5) Under the conditions of density ratio of 2.0 and blowing ratio of 2.0, the overall FCE of the optimized compound angled asymmetric fan shaped hole outperformed both the

experimentally optimized laidback fan shaped hole and the CFD optimized laidback fan shaped hole in previous studies by 1.3% and 8%, respectively.

Current results showed that the compound angled asymmetric laidback fan shaped holes could increase the FCE. Therefore, these results will be extended to the FCE in turbine blade cascade experiments in future research.

Author Contributions: Conceptualization, Y.R.J. and J.S.K.; methodology, Y.R.J. and J.Y.J.; software, Y.R.J. and J.Y.J.; validation, Y.R.J. and J.Y.J.; formal analysis, Y.R.J.; investigation, Y.R.J.; resources, J.S.K.; data curation, Y.R.J.; writing—original draft preparation, Y.R.J.; writing—review and editing, J.S.K. and Y.R.J.; visualization, Y.R.J.; supervision, J.S.K.; project administration, J.S.K.; funding acquisition, J.S.K. All authors have read and agreed to the published version of the manuscript.

Funding: This work was partly supported by Korea Institute of Energy Technology Evaluation and Planning (KETEP) grant funded by the Korea government (MOTIE) (Grant No. 20193310100050) and Basic Science Research Program through the National Research Foundation of Korea (NRF) funded by the Ministry of Education (Grant No. 2022R1A6A1A03056784).

Conflicts of Interest: The authors declare no conflict of interest.

Nomenclature

English symbols	
AR	area ratio of outlet to inlet [A_{outlet}/A_{inlet}]
D	hole diameter [mm]
DR	density ratio
I	emission intensity
L	hole length [mm]
M	blowing ratio
P	pressure
Greek symbols	
α	injection angle [°]
β	forward expansion angle [°]
γ	lateral expansion angle [°]
θ	compound angle [°]
η	film cooling effectiveness
ω	molecular weight
Subscripts	
air	air injection condition
blk	black condition
fg	foreign gas injection condition
fwd	forward expansion angle
lw	leeward
O_2	oxygen
ref	reference condition
ww	windward

References

1. Goldstein, R.J.; Eckert, E.R.G.; Burggraf, F. Effects of hole geometry and density on three-dimensional film cooling. *Int. J. Heat Mass Transf.* **1974**, *17*, 595–607. [CrossRef]
2. Sinha, A.K.; Bogard, D.G.; Crawford, M.E. Film-Cooling Effectiveness Downstream of a Single Row of Holes With Variable Density Ratio. *ASME J. Turbomach.* **1991**, *113*, 442–449. [CrossRef]
3. Pedersen, D.R.; Eckert, E.R.G.; Goldstein, R.J. Film cooling with large density differences between the free-stream and the leewardary fluid measured by the heat-mass transfer analogy. *ASME J. Heat Transf.* **1977**, *99*, 620–627. [CrossRef]
4. Chen, A.F.; Li, S.J.; Han, J.C. Film cooling for cylindrical and fan shaped holes using pressure-sensitive paint measurement technique. *J. Thermophys. Heat Transf.* **2015**, *29*, 775–784. [CrossRef]
5. Yang, X.; Liu, Z.; Feng, Z. Numerical Evaluation of Novel Shaped Holes for Enhancing Film Cooling Performance. *ASME J. Heat Transf.* **2015**, *137*, 071701. [CrossRef]

6. Dhungel, A.; Lu, Y.; Phillips, W.; Ekkad, S.V.; Heidmann, J. Film Cooling from a Row of Holes Supplemented with Antivortex Holes. *ASME J. Turbomach.* **2009**, *131*, 021007. [CrossRef]
7. Park, S.S.; Park, J.S.; Lee, S.H.; Moon, Y.G. Effect of Anti-Vortex Hole Angle on the Flat Plate Film Cooling Effectiveness. *KSFM J. Fluid Mech.* **2014**, *17*, 5–10. [CrossRef]
8. Khalatov, A.A.; Panchenko, N.A.; Borisov, I.I.; Severina, V.V. Numerical Simulation of Film Cooling with a Coolant Supplied Through Holes in a Trench. *J. Eng. Phys. Thermophys.* **2017**, *90*, 637–643. [CrossRef]
9. Wang, Y.; Wang, Z.; Wang, W.; Li, H.; Shen, W.; Cui, J. Predicting and optimizing multirow film cooling with trenches using gated recurrent unit neural network. *Phys. Fluids* **2022**, *34*, 045122. [CrossRef]
10. Rigby, D.L.; Heidmann, J.D. Improved Film Cooling Effectiveness by Placing a Vortex Generator Downstream of Each Hole. In Proceedings of the ASME Turbo Expo 2008, Berlin, Germany, 9–13 June 2008. GT2008-51361.
11. Deng, H.; Teng, J.; Zhu, M.; Qiang, X.; Lu, S.; Jiang, Y. Overall cooling performance evaluation for film cooling with different winglet pairs vortex generators. *Appl. Therm. Eng.* **2022**, *201*, 117731. [CrossRef]
12. Nasir, H.; Acharya, S.; Ekkad, S. Improved film cooling from cylindrical angled holes with triangular tabs: Effect of tab orientations. *Int. J. Heat Fluid Flow* **2003**, *24*, 657–668. [CrossRef]
13. Schmidt, D.L.; Sen, B.; Bogard, D.G. Film cooling With Compound Angle Holes: Adiabatic Effectiveness. *J. Turbomach.* **1996**, *118*, 807–813. [CrossRef]
14. Ekkad, S.V.; Zapata, D.; Han, J.C. Film Effectiveness Over a Flat Surface with Air and CO_2 Injection Through Compound Angle Holes Using a Transient Liquid Crystal Image Method. *ASME J. Turbomach.* **1997**, *119*, 587–593. [CrossRef]
15. Zamiri, A.; Chung, J.T. Large eddy simulation of compound angle effects on cooling effectiveness and flow structure of fan shaped holes. *Int. J. Heat Mass Transf.* **2021**, *178*, 121599. [CrossRef]
16. Huang, X.; Pu, J.; Zhang, T.; Wang, J.H.; Wu, W.L.; Wu, X.Y. Effect of length-to-diameter ratio on film cooling and heat transfer performances of simple and compound cylindrical-holes in transverse trenches with various depths. *Int. J. Heat Mass Transf.* **2022**, *185*, 122328. [CrossRef]
17. Bashir, M.H.; Shiau, C.C.; Han, J.C. Film cooling effectiveness for three-row compoound angle hole design on flat plate using PSP technique. *Int. J. Heat Mass Transf.* **2017**, *115*, 918–929. [CrossRef]
18. Natsui, G.; Claretti, R.; Ricklick, M.A.; Kapat, J.S.; Crawford, M.E.; Brown, G.; Kenneth, L. Experimental Evalution of Large Spacing Compound Angle Full-Coverage Film Cooling Arrays: Adiabatic Film Cooling Effectiveness. *J. Turbomach.* **2016**, *138*, 071001. [CrossRef]
19. Lee, K.D.; Kim, K.Y. Optimization of a cylindrical film cooling hole using surrogate modeling. *Int. C. Heat Transf.* **2009**, *55*, 362–380. [CrossRef]
20. Lee, K.D.; Kim, K.Y. Shape optimization of a fan shaped hole to enhance film-cooling effectiveness. *Int. J. Heat Mass Transf.* **2010**, *53*, 2996–3005. [CrossRef]
21. Seo, H.J.; Kang, Y.J.; Lee, H.C.; Kwak, J.S.; Park, J.S.; Lee, K.D. Optimization of the configuration of the laidback fan shaped film cooling hole with a lateral expansion angle of 10 degrees. *Appl. Therm. Eng.* **2019**, *153*, 379–389. [CrossRef]
22. Park, S.S.; Kim, Y.J.; Kwak, J.S. Film-Cooling Effectiveness of Antivortex Holes at Three Different Mainstream Turbulence Levels. *J. Propuls. Power* **2017**, *33*, 1562–1569. [CrossRef]
23. Abernethy, R.B.; Benedict, R.P.; Dowdell, R.B. ASME Measurement Uncertainty. *ASME J. Fluids Eng.* **1985**, *107*, 161–164. [CrossRef]
24. Bhattacharya, B. *Response Surface Methodology in Engineering Science: Publisher Location*, 23rd ed.; Intechopen: London, UK, 2021; pp. 2–21.
25. Brauckmann, D.; Wolfersdorf, J.V. Influence of Compound Angle on Adiabatic Film Cooling Effectiveness and Heat Transfer Coefficient for a Row of Shaped Film Cooling Holes. In Proceedings of the ASME Turbo Expo 2005, Reno-Tahoe, NV, USA, 6–9 June 2005. GT2005-68036.
26. Martin, J.D.; Simpson, T.W. Use of Kriging Models to Approximate Deterministic Computer Models. *AIAA* **2005**, *43*, 853–863. [CrossRef]
27. Myers, D.E. Matrix formulation of co-kriging. *J. Int. Assoc. Math. Geol.* **1982**, *14*, 249–257. [CrossRef]
28. Park, S.H.; Kang, Y.J.; Seo, H.J.; Kwak, J.S.; Kang, Y.S. Experimental optimization of a fan shaped film cooling hole with 30 degrees-injection angle and 6-hole length-to-diameter ratio. *Int. J. Heat Mass Transf.* **2019**, *144*, 118652. [CrossRef]